



# Full Lignin-Derived Electrospun Carbon Materials as Electrodes for Supercapacitors

Michael W. Thielke<sup>1</sup>, Stiven Lopez Guzman<sup>2</sup>, Jorge Pavel Victoria Tafoya<sup>1</sup>, Esteban García Tamayo<sup>2</sup>, Cristina Isabel Castro Herazo<sup>2</sup>, Omid Hosseinaei<sup>3</sup> and Ana Jorge Sobrido<sup>1\*</sup>

<sup>1</sup>School of Engineering and Materials Science, Queen Mary University of London, London, United Kingdom, <sup>2</sup>Escuela de Ingeniería, Universidad Pontificia Bolivariana, Medellín, Colombia, <sup>3</sup>RISE (Research Institutes of Sweden), Stockholm, Sweden

In the search for more sustainable energy storage devices, biomass-derived materials have been widely researched as carbon source for electrode applications. Here we present the processing of high molecular lignin, an abundant carbon rich biopolymer and byproduct of the pulp and paper industry, into freestanding nonwoven carbon fiber (CNFs) electrodes by using electrospinning. It is worth mentioning that no petrol-derived polymers that are usually included in the electrospinning of lignin, were employed in this work, making these electrodes more sustainable than common lignin-derived carbon electrodes. The effect of the carbonization temperature and oxygen plasma treatment in the electrochemical performance of the CNFs as electrodes for supercapacitors was studied. The upscaling of the processing of lignin into carbon electrodes was also explored by comparing a standard electrospinning set up with a needleless electrospinning equipment that enabled faster and higher throughput. The electrochemical performance of the CNFs increased after plasma treatment of the surface and the electrodes prepared using the standard set up exhibited the highest activity, achieving specific capacitances of up to 103.6 F g<sup>-1</sup>.

**Keywords:** Lignin, Electropinning, supercapacitor, Biomass, sustainability, needleless electrospinning, *in situ* Raman, plasma-modified carbon

## OPEN ACCESS

### Edited by:

Francisco Martin-Martinez,  
Swansea University, United Kingdom

### Reviewed by:

Vida Poursorkhabi,  
University of Guelph, Canada  
Francisco José García-Mateos,  
University of Malaga, Spain

### \*Correspondence:

Ana Jorge Sobrido  
a.sobrido@qmul.ac.uk

### Specialty section:

This article was submitted to  
Biomaterials,  
a section of the journal  
Frontiers in Materials

**Received:** 21 January 2022

**Accepted:** 21 March 2022

**Published:** 17 May 2022

### Citation:

Thielke MW, Lopez Guzman S, Victoria Tafoya JP, García Tamayo E, Castro Herazo CI, Hosseinaei O and Sobrido AJ (2022) Full Lignin-Derived Electrospun Carbon Materials as Electrodes for Supercapacitors. *Front. Mater.* 9:859872. doi: 10.3389/fmats.2022.859872

## INTRODUCTION

The increasing global energy demand and the urgency to reduce the worldwide carbon footprint is an indication of the need to develop more efficient energy storage systems. Due to the finite amount of fossil fuels, as well as the heavy environmental pollution and impact, which results from the extraction and the combustion of fossil fuels, sustainable alternatives for energy harvesting and storage systems are urgently needed. Electrochemical double-layer capacitors (EDLCs) are energy storage devices that possess high-power density, fast charge/discharge rate, and excellent cyclability. Due to their storage mechanism, based on electrostatic interactions between ions and the electrode surface, lifetime and stability are much higher than secondary batteries, exhibiting higher power capabilities but lower energy density (Guan et al., 2016). These properties make EDLCs well suited for high power demand applications, isolated electronic systems with low maintenance, grid stabilization, or to incept power peaks to protect other batteries as a power buffer (Naseri et al., 2022). Carbon-based materials are ideal electrodes for EDLCs as they can be highly conducting and exhibit large surface area as well as high porosity (Abioye and Ani, 2015). Another advantage of

carbon electrodes is the possibility to obtain them from sustainable biomaterials, such as biomass waste (Azam et al., 2021). Among the available techniques to process biomass into electrodes, electrospinning is an ideal technique, as it enables the production of freestanding electrodes consisting of nonwoven carbon fibers with remarkably high surface to volume ratio (Li et al., 2021; Tiwari et al., 2021). Electrospinning is a simple method that uses a high voltage to create an electric field on a polymer solution or melt. The physical entanglement of the polymer chains and the evaporation of the solvent or the freezing of the melt allows the formation of fibers in the nanometer scale, with a broad field of applications, including energy harvesting (Laudenslager et al., 2010; Szewczyk et al., 2020) and storage (Mao et al., 2013; Li et al., 2016; Sun et al., 2021).

Out of the synthetic polymers, polyacrylonitrile (PAN) has been employed for the fabrication of high-performance electrospun carbon fibers, due to its high melting point, solubility in organic solvents, and the ability to form stable cyclic carbon structures. However, the use of PAN displays major drawbacks associated with the high energy demand and long processing time. Moreover, PAN is a synthetic polymer that derives from petroleum, and its use should be avoided. From a sustainable perspective, the use of biomass for creating carbon structures is a promising step towards full sustainability (Herou et al., 2018). The electrospinning of biopolymers has been widely reported in the literature, including cellulose and cellulose derivatives (Frey, 2008), chitin (Min et al., 2004), and lignin (Schlee et al., 2019; Svinterikos et al., 2020; Wen et al., 2021). Lignin is the second most abundant biopolymer worldwide, and it is a side product of the pulp and paper industry, therefore a relatively cheap and available in large quantities worldwide. Due to its high carbon content, electrospun lignin is a suitable candidate as precursor for carbon materials and has the potential to replace fossil derived polymers such as PAN, which has been the focus of a number of reviews (Kumar et al., 2019; Poursorkhabi et al., 2020; Svinterikos et al., 2020). Due to its intrinsic nature, lignin, as well as other biopolymers, exhibit a broad distribution of molecular weight, which is the reason why the majority of published works on electrospun lignin, blend lignin with other, mainly petroleum based polymers, such as PVA (Lai et al., 2014; Ago et al., 2016; Ma et al., 2016), PEO (Hu et al., 2014; Wang et al., 2017), PVP (Ma et al., 2018), or PAN (Choi et al., 2013; Lei et al., 2017; Perera Jayawickramage et al., 2019) in order to obtain a suitable entanglement for the fabrication of stable fibers as precursor for carbon fibers.

In this study, we have used an alternative approach for enabling electrospinning. Instead of blending the polymer, we used a high molecular fraction of lignin to produce freestanding carbon fibers without any additional polymer for carbon fibers to achieve full biomass derived carbon fibers, without any influence of active or passive additives. Although, this method is very intensive regarding solvent consumption, the long-term reusability of solvent, as well as the exclusion of petroleum based synthetic polymers, makes this method a viable option towards a fully sustainable device. To compare the influence of

the carbonization temperature, carbon fibers were treated at three different temperatures (850°C, 1000°C, and 1150°C). As previous studies have shown, the selected parameters during carbonization influence the specific capacitance of the material such as performing a stabilization process before carbonizing the material under inert atmosphere, achieving capacities of up to 50 F/g at a 2 A g<sup>-1</sup> current (Lai et al., 2014). Another more direct route stabilizes the material under vacuum at 60°C for 24 h, before performing a two-step carbonization process obtaining a capacity of 216.8 F g<sup>-1</sup> at 1 A g<sup>-1</sup> (Wang et al., 2018). Berenguer *et al* explored the effect of the heating rate in lignin, showing that a correct value in this parameter would lead to an interconnected fiber structure or to a loose structure, while the fiber diameter remains constant. To obtain a connected structure more suitable for supercapacitors, they employed Alcell lignin with pure ethanol as electrospinning solution obtaining a capacity of 47 F g<sup>-1</sup> at 1 A g<sup>-1</sup> after 50.000 cycles (Berenguer et al., 2016). Carbon electrodes applications are limited by their low electric capacitance, regular stability, and poor specific capacitance. Because of that, the addition of metallic oxide is shown as a good alternative to increase their performance to make them more suitable for our interest. One example is the use of iron nanostructures in the lignin fibers to increase the specific capacity and capacitance retention of the lignin electrode (216 F g<sup>-1</sup> at 0.1 A g<sup>-1</sup>) (Butnoi et al., 2021). García-Mateos *et al* uses additional H<sub>3</sub>PO<sub>4</sub> in an Alcell lignin-ethanol solution to induce an oxygen-based activation process during carbonization and increase the surface area to 2340 m<sup>2</sup> g<sup>-1</sup> reaching a specific capacity of 50% (CP: ~45 F g<sup>-1</sup> at 2 A g<sup>-1</sup>) (García-Mateos et al., 2020). In this study, oxygen plasma treatment was applied to increase the hydrophilic character of the produced carbon fibers surface, which favored wettability and hence the access of the KOH electrolyte to the fiber surface. Here, we have also explored the scalability of the process by producing lignin-derived carbon fibers using a larger-scale needleless electrospinning equipment.

## MATERIALS AND METHODS

### Preparation of High Molecular Weight Lignin

Softwood Kraft lignin was obtained from a LignoBoost process (Bäckhammer, Sweden). A sequential solvent extraction was conducted to produce the suitable lignin fraction for electrospinning of lignin. The solvent extraction method was a simplified version (Moerck et al., 1987), where 1 kg lignin ( $M_n = 1300 \text{ g mol}^{-1}$ , PDI 3.5, UV detector at 280 nm, polystyrene calibration) was extracted in 10 L methanol at room temperature while stirring for 2 h, filtrated, and extracted using a 7/3 v/v mixture of methanol and methylene chloride (1:10 solid to liquid ratio, room temperature, 4 h). The extract solution was filtered and lignin from the filtrate was dried under lowered pressure. The isolated lignin ( $M_n = 8600 \text{ g mol}^{-1}$ , PDI 2.8) was further dried under vacuum at 80°C for 12 h with a yield of 42.5%. (FT-IR data can be found in **Supplementary Figure S1**).

## Electrospinning

Standard electrospinning was performed using a solution of 45.5 wt% lignin in DMF. A blunt 21G needle was employed with a tip-to-collector distance of 15 cm to a metal plate to collect the fibers as a non-woven mat. A voltage of 23.0 kV was used at a flow rate of 0.3 ml/h, with a total volume of 1 ml solution. To support an efficient evaporation of the solvent, the atmosphere around needle tip was flushed with a stream of air with a low relative humidity of ~0%. Samples prepared using this approach were labelled as “ES”.

Needleless electrospinning was performed in an Elmarco<sup>®</sup> Nanospider electrospinning equipment with an identical lignin solution. The distance of the high voltage and the grounded collector was set to 200 mm at a voltage of 60 kV. The 10 ml cartridge with an 8 mm diameter hole was set between the range of 50 and 300 mm with a cartridge period of 2.5 s and a waiting period of 7.5 s. Samples prepared using this equipment were labelled as “NS”. Due to the Nanospider setup, supporting the electrospinning process with flowing air to improve the evaporation rate was not possible for the NS samples.

## Physical and Chemical Characterization

Field emission scanning electron microscopy (SEM, FEI Inspect F50<sup>®</sup>) was used to study the morphology and surface structure of the obtained binder-free electrospun lignin fibers. X-ray photoelectron spectroscopy (XPS, Thermo Scientific, Nexsa<sup>®</sup>) was used to investigate chemical composition. Surface area measurements (BET) were conducted using N<sub>2</sub> as adsorbate in a Nova Quantachrome<sup>®</sup> instrument. X-ray diffractometry was used to investigate crystallinity and structural information of the electrospun mats using a Siemens D5000<sup>®</sup> powder diffractometer with a  $\theta/2\theta$  geometry in reflection mode equipped with a Cu K $\alpha$  source with a wavelength of ~1.54 Å. For further structural and chemical analysis, Raman spectroscopy (Renishaw in Via<sup>®</sup>, 442 nm, and objective lens 50 ×) was employed to calculate defect/graphitic ratio ( $I_D/I_G$ ).

## Electrode Preparation

The carbon nanofibers (CNFs) were obtained *via* activation of the as-spun fibers at 250°C in a preheated oven for 2 h (DSC with heating profile can be found in **Supplementary Figure S2**) in air, followed by carbonization under nitrogen atmosphere at either 850°C, 1000°C, or 1150°C for 4 h and a heating rate of 5°C min<sup>-1</sup>. The plasma treatment of the surface of the CNFs was performed in a radiofrequency (13.56 MHz) plasma reactor. The pressure was maintained ~1.2 mbar in air, with a power ~10 W for 20 s to increase the hydrophilicity of the lignin derived CNFs.

## Electrochemical Measurements

To evaluate the supercapacitance of the obtained electrospun fibers, cyclic voltammetry (CV), chronopotentiometry (CP) and electrochemical impedance spectroscopy (EIS) were performed using a supercapacitor assembly in a quick assembly split cell (MTI Corporation, EQ-HSTC<sup>®</sup>, 20 mm diameter). The full-cell assembly was connected to a Biologic SP300<sup>®</sup> potentiostat to perform the electrochemical experiments. For the physical assembly of the supercapacitor, two disks of ~1.2 cm were cut

from the electrospun mat using a punch and weighted. The obtained disks were soaked in a 6 M KOH solution overnight prior the electrochemical experiment. Subsequently, each soaked disk was placed on top of a graphite current collector disk with same diameter. Finally, a wettened glass-fiber disk used as separator with 2 ml of 6 M KOH solution and same diameter was placed between the two electrodes and compressed using the EQ-HSTC<sup>®</sup> cell. CV were performed for all the evaluated samples at different scan rates: 5, 10, 50, 100, 200, 500 and 1000 mV s<sup>-1</sup>. Then, a galvanostatic charge-discharge test was performed using an applied gravimetric current density of 0.5 A g<sup>-1</sup>, for 100 complete charge-discharge cycles. EIS was conducted to study mass transport and charge transport losses. For this, the electrochemical cell potential was fixed at 0.4 V with a perturbation of 5 mV (0.003 V<sub>rms</sub>). EIS spectra were recorded using a frequency window between 100 kHz and 100 mHz recording 10 points per decade. Additionally, CVs were measured at 1, 2, 5, 10 and 20 mV s<sup>-1</sup> scan rates for the best performing sample to precisely determine its double layer capacitance. In addition, charge-discharge cycles using supplementary gravimetric current densities were recorded using 0.25, 0.5, 0.75, 1, 2 and 4 A g<sup>-1</sup>, running 10 complete charge-discharge cycles. Finally, to assess the cyclability of the best performing material, 6 000 charge-discharge cycles were recorded using a gravimetric current density of 1 A g<sup>-1</sup>. Finally, *in-situ* Raman characterization of the electrospun mats were carried out with an *in-situ* Raman electrochemical cell (MTI Corporation, EQ-STC-Raman<sup>®</sup>). This experiment was carried by holding the applied potential of the supercapacitor assembly until reaching equilibrium before the acquisition of spectrum (**Supplementary Figure S3**). This experiment was performed at an initial applied potential of 0.25 V, increasing the potential with equidistant steps of 100 mV until reaching 0.75 V for the charging process of the electrochemical device. For the discharge, same procedure was performed by decreasing the applied potential from 0.75 to 0.25 V.

## RESULTS AND DISCUSSION

In order to assess the scaling-up of the production of carbon fibers from pure lignin using electrospinning, a home-built lab-scale electrospinning set up (ES samples) was compared to a larger scale commercial needleless electrospinning setup (Elmarco<sup>®</sup> Nanospider, NS samples) (**Figure 1**).

Full biomass-derived carbon fiber mats were produced by electrospinning high molecular fraction of lignin. The fibers (ES and NS) retained their morphology after thermal treatment, with a decrease in diameter with increasing temperature (**Figure 2**). Similar to a previously report of that uses a Nanospider setup for lignin on a comparable sample (Mikeš et al., 2021) a significant higher voltage was needed in order to overcome the surface tension and form stable streams to obtain an electrospun lignin fiber mat.

SEM analysis revealed significant differences for both set of samples. A larger diameter and a narrower distribution (1000 ± 104 nm) were observed for the ES fibers, compared to the NS

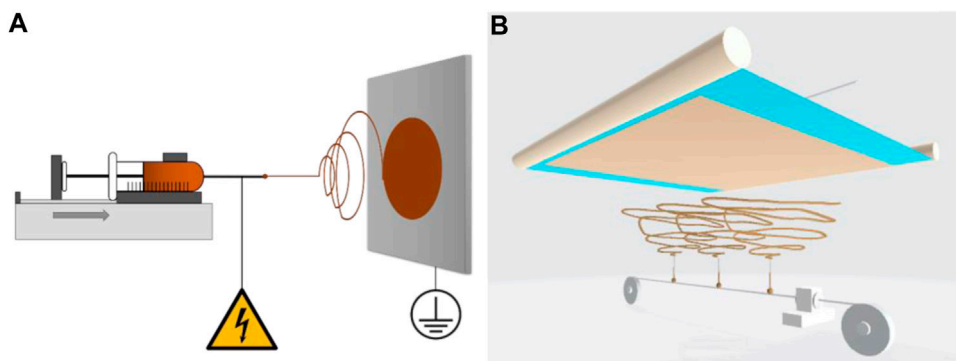


**FIGURE 1 | (A)** Standard electrospinning setup: A constant flow (0.3 ml/h) of a lignin solution is pumped through a blunt needle, which is connected to a high voltage. The solution forms a Taylor cone towards the grounded collector. The evaporation of the solvent and the entanglement of the polymers lead to the formation of electrospun fibers. **(B)** Nanospider electrospinning setup: The solution is loaded into a cartridge that periodically moved along a wire, which is connected to high voltage supply. Through a hole in the cartridge, the containing solution is deposited onto the wire and forms droplets onto the wire surface, which then spray towards a second grounded wire parallel to the high voltage wire in a defined distance. Each droplet forms a Taylor cone, leading to the formation of a jet of fibers that deposit onto the target in the form of nonwoven fibers. Between the two wires, a mesh is placed in order to collect the resulting fibers.

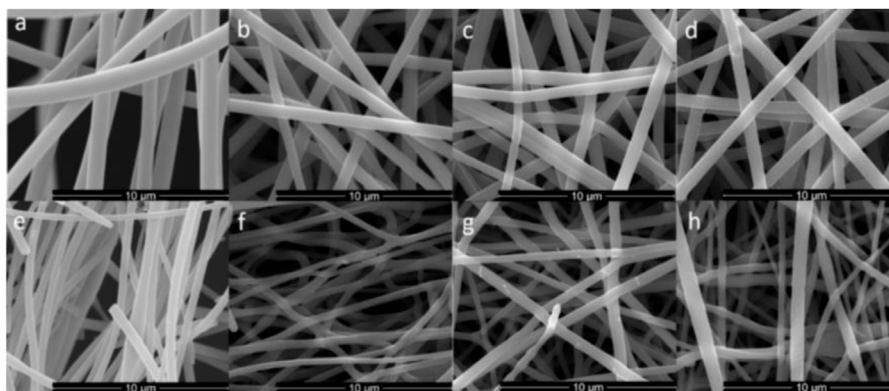


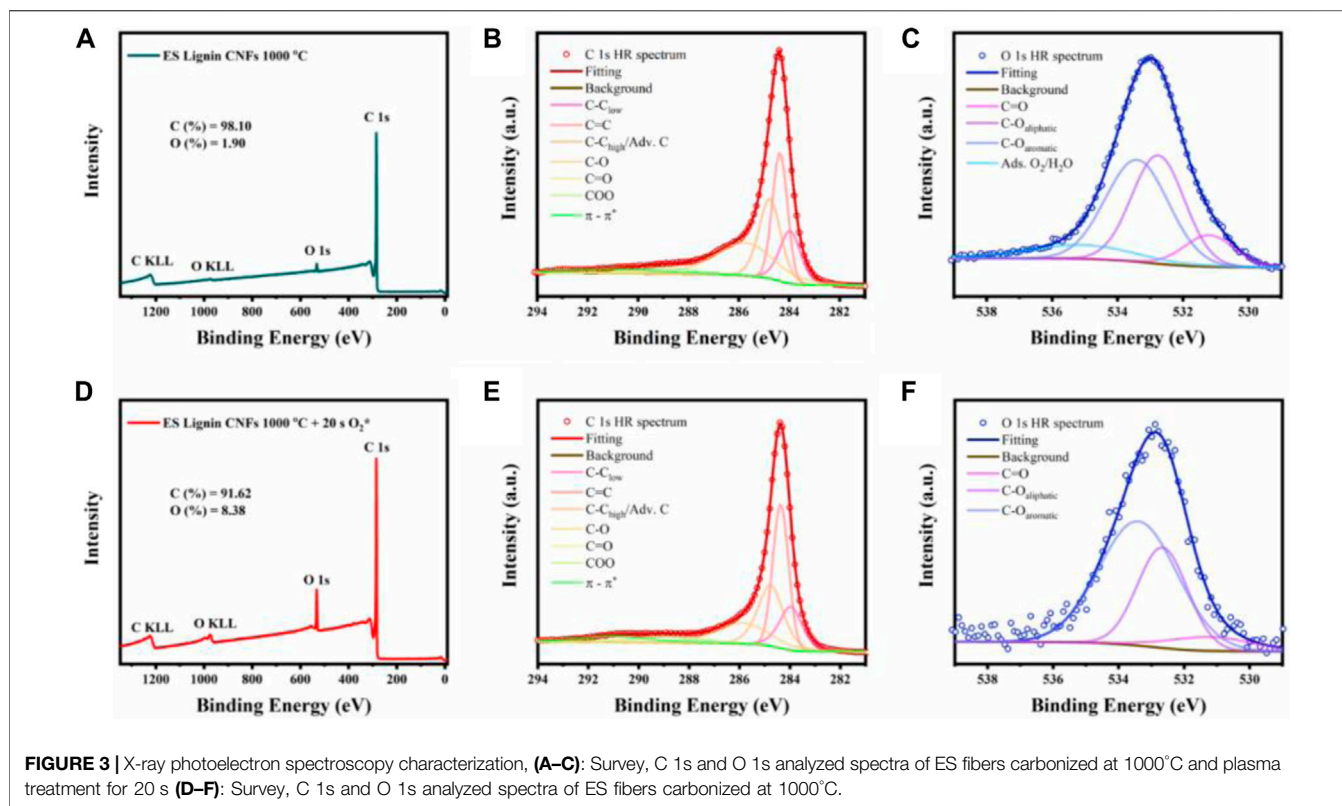
**FIGURE 2 | (A–D)** SEM of ES fibers: **(A)** as-spun, **(B)** after carbonization at 850°C **(C)** after carbonization at 1000°C, and **(D)** after carbonization at 1150°C. **(E–H)** SEM of NS fibers: **(E)** as-spun, **(F)** after carbonization at 850°C, **(G)** after carbonization at 1000°C, and **(H)** after carbonization at 1150°C. The average fiber diameter was determined *via* ImageJ by taking the diameter of at least 150 fibers per sample.

**TABLE 1 |** Fiber diameters and BET surface area results for the as-spun and carbonized ES and NS fibers.

Sample	Diameter (nm)	BET ( $\text{m}^2 \text{g}^{-1}$ )
ES—as electrospun lignin	1000 ± 105	7.2
ES—850°C	744 ± 98	700
ES—1000°C	640 ± 144	1124
ES—1150°C	704 ± 69	133
NS—as electrospun lignin	509 ± 124	8.7
NS—850°C	484 ± 176	557
NS—1000°C	614 ± 93	73.1
NS—1150°C	521 ± 169	61.2

fibers ( $510 \pm 123$  nm). Additionally, the needleless approach led to partially fused fibers (seen in detail in **Supplementary Figure S5**), attributed to the incomplete evaporation of the solvent. The average diameters and BET of the electrospun fibers before and

after the carbonization are shown in **Table 1**. The diameter of the fibers decreased significantly upon thermal treatment in the case of the ES, from  $\sim 1000$  nm for the as-spun lignin fibers to  $\sim 650$ – $750$  nm for the thermal treated. In the case of the NS samples, the fiber diameter of the as-spun lignin fibers is significant smaller than the ES fibers, decreasing from  $\sim 1000$  to  $\sim 500$  nm. NS samples did not appear to undergo significant shrinking in the fiber diameter upon thermal treatment, with an average value of  $\sim 500$ – $600$  nm for all the NS samples, which could also be an indication of residual trapped solvent within the fibrous structure. The higher voltage and therefore stronger electric field needed to obtain stable fibres from the Nanospider setup could contribute to the overall smaller diameter of the produced fibers using this approach. The BET surface area significantly increased after the carbonization, as expected, particularly in the case of the ES fibers, from  $7 \text{ m}^2 \text{g}^{-1}$  for the as-spun material to  $1124 \text{ m}^2 \text{g}^{-1}$  for the material treated at

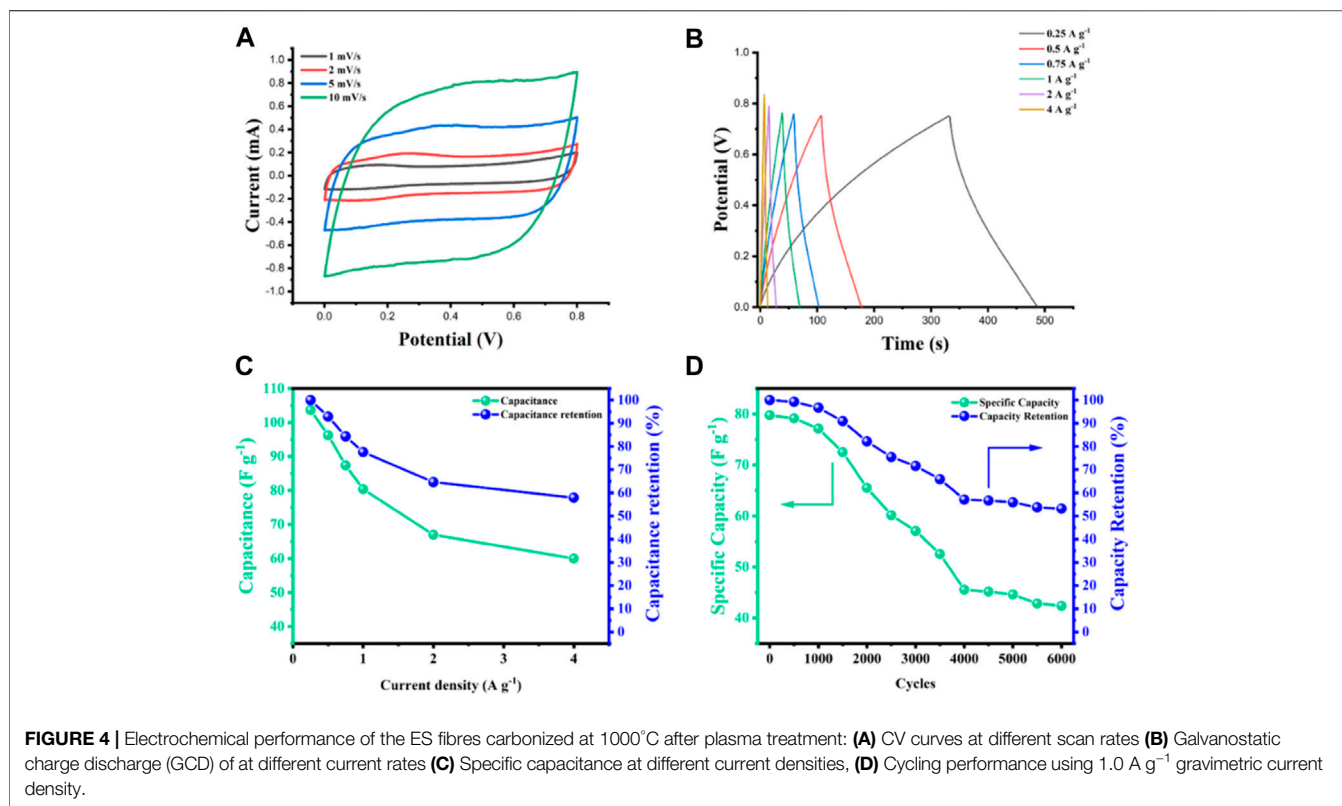


1000°C. Surprisingly, the fibers treated at the highest temperature, 1150°C, exhibited a lower BET surface area, of 133 m<sup>2</sup> g<sup>-1</sup>. In the case of the NS materials, a maximum BET surface area of 557 m<sup>2</sup> g<sup>-1</sup> was observed for the sample carbonized at the lowest temperature, 850°C, decreasing dramatically upon heating with values of BET surface area, decreasing to 73.1 m<sup>2</sup> g<sup>-1</sup> and 61.2 m<sup>2</sup> g<sup>-1</sup> for 1000 and 1150°C, respectively. This is probably associated with the appearance of fused fibers. The pore size distributions of each samples can be found in the (Supplementary Figures S3). Interestingly, the sample with higher BET surface area, ES 1000°C exhibited a broader pore size distribution with pores ranging from ~2 to 35 nm. These results highlight the challenges associated with upscaling processes in terms of optimization of parameters to obtain reproducible results in larger scale set up.

The carbonization of the fibers was studied *via* XRD (Supplementary Figure S6), with similar result for all the samples. A small broad peak around 20° corresponding to C(002) and an additional contribution corresponding to C(101) around 45° were observed. In addition to that, Raman measurements were performed (Supplementary Table S1). ES and NS samples exhibited similar I<sub>D</sub>/I<sub>G</sub> ratio, between 0.75 and 0.81, with the NS fibers presenting slightly lower values, suggesting a slight decrease in defect concentration for the NS materials.

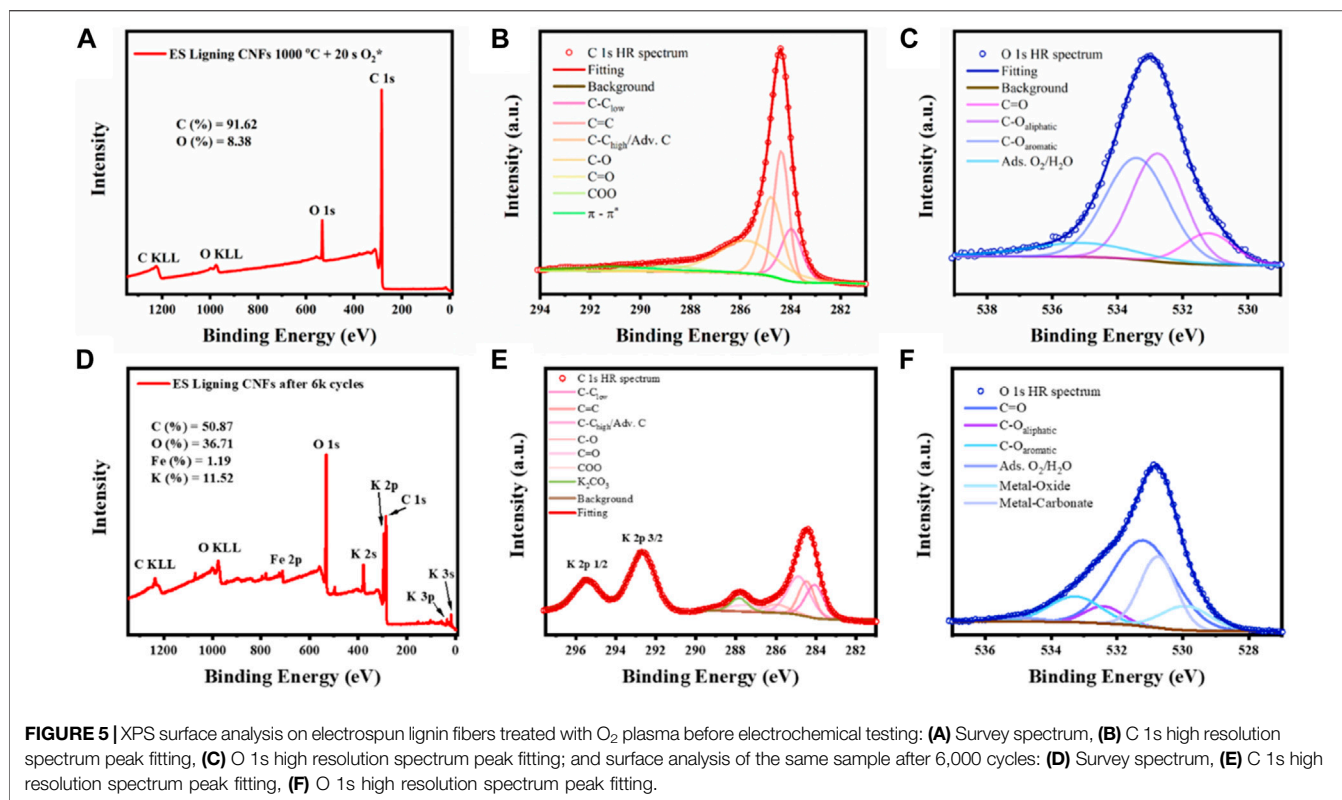
XPS was used to determine the average chemical environment of the surface of the electrospun mats before and after plasma treatment. Figure 3 shows the analyzed surveys, C1s and O1s spectra for the ES fibers carbonized at 1000°C with and without plasma treatment. The effect of plasma treatment was also

evaluated for the NS fibers using XPS (Supplementary Figure S7). The survey spectra analysis (Figures 3A,D) revealed a higher O content when plasma treatment was applied, increasing from ~2 at% to ~10 at%, attributed to the increase in C-OH groups. C1s peak fitting (Figures 3B,E) was performed placing the peak center of C1s ~ 284.4 eV, corresponding to C=C bonding (Smith et al., 2016). Both samples (with and without plasma treatment) exhibited a dominant C=C peak correlated with a graphitic-like structure. Additionally, contributions corresponding to C-C low binding energy defective domains (~284 eV) and C-C high binding energy defective domains which overlapped with adventitious C (~284.8 eV) were also observed (Smith et al., 2016). For both samples, C 1s peak fitting presented a dominant signal around the tail feature of the spectra, corresponding to C-O (~286.2 eV), and a small contribution from C=O (~287.4 eV) and COO (~288.9 eV). Specifically, for the ES carbonized at 1000°C without plasma treatment, the contribution of the C from C-O increases to 16.1 at%, whereas for the plasma treated sample after carbonization the atomic percentage of this type of bonding increases up to ~24.3 at%. This confirms that the oxygen plasma treatment produces preferentially alcohol functional groups on the surface of the fibers. Additionally, O1s high resolution spectra fitting (Figures 3C,F) supports the preferential formation of C-O aliphatic groups (~532.8 eV) which correlates with alcohol surface functional groups (Smith et al., 2016). The increase of C-OH surface functionalities promotes the formation of the double-layer capacitance of the material, correlated with higher valence electron population on the surface of the electrode (Li et al., 2020).



The electrochemical performance for the CFs were evaluated in a two-electrode system in 6 M KOH aqueous solution. **Figure 4** shows the results for the best performing sample, ES carbonized at 1000°C with plasma treatment. Electrochemical measurements confirmed that plasma treatment had a positive effect on the electrochemical performance of the fibers, changing from symmetrical triangles in the GCD for pure lignin derived carbon fiber samples, to non-symmetrical curved triangles in GCD (**Supplementary Figure S8**). The change in the performance is associated to the increased presence of oxygen (C-OH groups) on the carbon fiber surface, as confirmed in XPS analysis, contributing to the presence of a pseudo capacitance behavior (Hérou et al., 2021) and an enhancement of the overall storage performance (Andreas and Conway, 2006). In particular, the electrochemical performance of the ES-1000°C electrode improved remarkably after plasma, attributed to the higher BET surface area that could also accommodate more C-OH functional groups. The NS fiber electrodes did not increase significantly their performance after plasma treatment. **Figure 4A** shows that the CV curves for low scan rates of the material exhibit a quasi-rectangular shape indicating the presence of the double layer capacitance phenomenon. There is an evident change in the shape of the CV curve with increasing scan rate, from quasi-rectangular to ovoidal, which can be correlated with the increase in charge transfer resistance of the material and presence of faradaic-like processes, caused by the presence of additional C-OH groups on the surface which in turn, also increases of the wettability and electron transport of the system (Han et al., 2013). The GCD (**Figure 4B**) shows no

obvious IR drops. Instead, the presence of side reactions indicates that the system is not completely reversible, resulting in a higher charging time than the discharging time. Only a portion of the charge that passed during the charging period is released during the discharge (Chen, 2013), which is attributed to the higher amount of oxygen rich groups in the material after plasma treatment. Further studies need to be done to define the real influence of the faradaic-like processes in the system (Guan et al., 2016). Specific capacitances of 103, 96, 87, 80, 67, 60 F g<sup>-1</sup> for 0.25, 0.5, 0.75, 1, 2 and 4 A g<sup>-1</sup>, respectively, were obtained analyzing our supercapacitor as EDLC. These values are higher than previous reported electrospun carbon fiber using pure lignin as a precursor material (Lai et al., 2014; Berenguer et al., 2016; García-Mateos et al., 2020). **Figure 4C** shows the evaluation of different current densities and the influence in the specific capacitance values. An increase in current from 0.25 A g<sup>-1</sup>–4 A g<sup>-1</sup> led to a capacity reduction of 58%. Remarkably, an outstanding capacity retention of 97% was achieved over the 1000 first cycles, which then faded to 82% after 2000 cycles (**Figure 4D**), a phenomenon that has been reported for other lignin-based electrodes (Wang et al., 2018). After 6000 cycles, a capacity fade of 53% was obtained, which could be attributed to structural changes of the material during cycling (Krittayavathananon et al., 2017). The system maintained an energy density of 2.65 Wh kg<sup>-1</sup> at a power density of 60.24 W kg<sup>-1</sup> (**Supplementary Figure S12**). EIS data revealed insightful information about the resistivity and interaction electrode/electrolyte, with the best performing samples exhibiting the lowest internal resistivity (5.84 Ω), (**Supplementary Figure**



S13), attributed to its high BET surface area, which enabled an easier diffusion of the ions within the material at a high rate (Suda et al., 2017). The value for the gravimetric capacitance was calculated from GCD curves using the equation (Jeong et al., 2020)

$$C = \frac{4I\Delta t}{m\Delta V}$$

In this case, C is the gravimetric capacitance (F g<sup>-1</sup>), I the discharge current (A),  $\Delta t$  is the discharge time in the selected potential(s), m the mass of the electrode (g) and  $\Delta V$  the difference of potential during discharge (V).

XPS (Figure 5) and SEM (Supplementary Figure S2) measured after cycling confirmed the degradation of the fibers. After electrochemical testing and 6,000 cycles of accelerated degradation testing, it was found that the surface of the material changed substantially. C 1s line shows a clear enhancement of the signal related to sp<sup>3</sup> and defective carbon domains (284.8 and 284 eV) and the appearance of a peak centered at 287.9 eV reported to be relevant to K<sub>2</sub>CO<sub>3</sub> species on the surface of the fibers. This was confirmed by the presence of K 2p<sub>3/2</sub> peak centered at 292.3 eV related to K<sub>2</sub>CO<sub>3</sub> (Iranmahboob et al., 2001). Additionally, iron was detected during survey spectrum showing a clear Fe 2p<sub>3/2</sub> peak centered at ~ 711.5 eV suggesting the dominant presence of oxidized Fe<sup>3+</sup>. The presence of iron can be explained by the polarization processes during charge-discharge testing, resulting in Fe leaching from the stainless-steel collector. Furthermore, O 1s confirmed the formation of metal oxides, Fe-O and K-O, and

metal carbonates with those peaks centered at ~ 530 and ~531 eV respectively (Dupin et al., 2000). Formation of these crystals on the surface of the electrospun fibers contributed to a significant decrease of the double layer capacitance of the material. Surface area decreased due the coverage of the surface of the fibers, making the diffusion of ions and polarization of electrodes more difficult.

For further investigation of structural changes on the surface of the material during electrochemical testing, *in-situ* Raman measurements were carried out. As a reference, an *ex-situ* Raman spectrum of the material was measured (Figure 6A). For the *in situ* measurements, a static potential of 0.25 V was applied to the cell for 15 min recording the chronoamperometric response. Once the measured current reached equilibrium, the Raman spectrum was recorded. This process was repeated increasing the applied potential with a  $\Delta E = 0.1$  V between each step, until reaching 0.75 V. This process intended to mimic a galvanostatic charging process. Similarly, the discharge process was also conducted and the Raman spectra measured from 0.75 to 0.25 V. As shown in Figure 6B, clear increase on the  $I_d/I_g$  ratio is observed during charging conditions until reaching the maximum applied potential of 0.75 V. This spectrometric response indicates an increase in concentration of the defective and amorphous carbon domains of the electrospun fibers (Vicentini et al., 2021). Nonetheless, Raman spectra D and G bands can reasonably be composed by specific bands corresponding to different vibrational modes of a variety of C symmetries (Sadezky et al., 2005). By

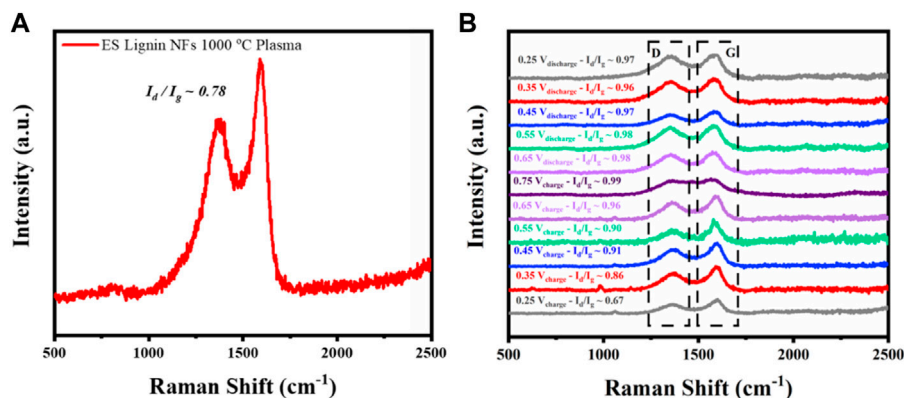


**FIGURE 6 | (A)** *Ex-situ* and **(B)** *in-situ* Raman spectra recorded under electrochemical potentiostatic conditions between 0.25 and 0.75 V ( $\Delta E = 0.1$  V).

inspection of the evolution of the spectra, the apparent increase of the D to G ratio is not only correlated with the  $D_1$  vibrational mode ( $\sim 1350\text{ cm}^{-1}$ ) of disordered graphitic lattice with an  $A_{1g}$  symmetry. Also, with an increase of the  $D_3$  vibrational mode ( $\sim 1500\text{ cm}^{-1}$ ) related with amorphous C domains and  $D_4$  band ( $\sim 1200\text{ cm}^{-1}$ ) which is associated with disordered graphitic domains as well as with ionic impurities on the surface of the material (Sadezky et al., 2005). The diffusion and proximity of ions between anode and cathode interfaces close the proximity to the Debye length shows an expected increase of the D to G ratio, also in agreement with ab-initio calculations published by Vicentini et al. Clearly, this can be correlated to the decrease on the polarization capability of the electrodes showing a significant negative effect on the double layer capacitance after many cycles (Figures 4C,D) (Vicentini et al., 2021). These findings provide insight on the possible causes on the decrease of capacitance retention, since the surface of the electrode is clearly modified upon charge/discharge cycles. This is possibly because alignment of ionic species on the surface of the material that derive on the increasing on intensity of  $D_4$  band and surface degradation.

## CONCLUSION

Pure and binder-free lignin derived electrospun carbon fibers were obtained by two different electrospinning techniques (standard lab scale and a larger scale/needleless set ups) and carbonized at temperatures from 850 to 1150°C, to obtain free standing electrodes. A comparison of both electrospinning set ups showed significant differences between the fibers obtained. While the standard set up produced uniform fibers, the larger scale/needleless configuration formed partially fused fibers of smaller diameter, and overall also a lower BET surface area. This was associated to the higher voltage needed to initiate the formation of fibers with the needleless set up and to the inefficient evaporation of the solvent. These results underline the challenges of upscaling this process, and different approach in terms of spinning solution and thermal treatments need to be further investigated to produce comparable materials.

The electrospun fibers were modified using oxygen plasma treatment to improve the wettability and increase the interfacial interaction between the electrolyte and the electrospun mat. The plasma modification technique for freestanding lignin fibers is a promising approach to increase the electrochemical performance for supercapacitors, but since the presence of the oxygen functional groups has a direct impact on the obtained results, we make a transition from a symmetric double layer mechanism to a pseudo-capacitor one. The ES fibers carbonized at 1000°C with plasma surface treatment showed a specific capacity of  $103.64\text{ F g}^{-1}$  at a current density of  $0.25\text{ A g}^{-1}$ , with mass per surface unit of  $2.212\text{ mg cm}^{-2}$ , high-capacity retention of 97% in the first 1000 cycles but a significant decrease in the final 6000 cycle is observed. A change in the surface properties of the material was confirmed by postmortem analysis of the cycled electrodes by XPS and SEM, that derived into a faradaic process caused by the presence of the other components in the surface and by the change in the fibers arrangement that could difficult the diffusion of ions within the electrode. In addition, an *In-situ* Raman characterization under electrochemical conditions provided further insight on the surface modification of the material suggesting the alignment and staking of multiple ionic species on the surface of the fibers. This also suggests that under strong alkaline conditions amorphous carbon domains are created due to the chemical decomposition of the carbonaceous matrix of the fibers.

## DATA AVAILABILITY STATEMENT

The original contributions presented in the study are included in the article/Supplementary Material, further inquiries can be directed to the corresponding author.

## AUTHOR CONTRIBUTIONS

MT, SL and JV contributed to the experiments and overall writing of the manuscript. EG and CC contributed to the discussion of the results and manuscript. OH contributed with the lignin samples

and discussion of results. AS contributed to the overall supervision of the project, discussion of results and writing of the manuscript.

## FUNDING

JV acknowledges the financial support given by CONACyT during his PhD in Queen Mary University of London. AS

## REFERENCES

- Abioye, A. M., and Ani, F. N. (2015). Recent Development in the Production of Activated Carbon Electrodes from Agricultural Waste Biomass for Supercapacitors: A Review. *Renew. Sust. Energ. Rev.* 52, 1282–1293. doi:10.1016/j.rser.2015.07.129
- Ago, M., Borghei, M., Haataja, J. S., and Rojas, O. J. (2016). Mesoporous Carbon Soft-Templated from Lignin Nanofiber Networks: Microphase Separation Boosts Supercapacitance in Conductive Electrodes. *RSC Adv.* 6, 85802–85810. doi:10.1039/c6ra17536h
- Andreas, H. A., and Conway, B. E. (2006). Examination of the Double-Layer Capacitance of an High Specific-Area C-Cloth Electrode as Titrated from Acidic to Alkaline pHs. *Electrochimica Acta* 51, 6510–6520. doi:10.1016/j.electacta.2006.04.045
- Azam, M. A., Ramli, N. S. N., Nor, N. A. N. M., and Nawi, T. I. T. (2021). Recent Advances in Biomass-derived Carbon, Mesoporous Materials, and Transition Metal Nitrides as New Electrode Materials for Supercapacitor: A Short Review. *Int. J. Energ. Res* 45, 8335–8346. doi:10.1002/er.6377
- Berenguer, R., García-Mateos, F. J., Ruiz-Rosas, R., Cazorla-Amorós, D., Morallón, E., Rodríguez-Mirasol, J., et al. (2016). Biomass-derived Binderless Fibrous Carbon Electrodes for Ultrafast Energy Storage. *Green. Chem.* 18, 1506–1515. doi:10.1039/c5gc02409a
- Butnoi, P., Pangon, A., Berger, R., Butt, H.-J., and Intasanta, V. (2021). Electrospun Nanocomposite Fibers from Lignin and Iron Oxide as Supercapacitor Material. *J. Mater. Res. Tech.* 12, 2153–2167. doi:10.1016/j.jmrt.2021.04.017
- Chen, G. Z. (2013). Understanding Supercapacitors Based on Nano-Hybrid Materials with Interfacial Conjugation. *Prog. Nat. Sci. Mater. Int.* 23, 245–255. doi:10.1016/j.pnsc.2013.04.001
- Choi, D. I., Lee, J.-N., Song, J., Kang, P.-H., Park, J.-K., and Lee, Y. M. (2013). Fabrication of Polyacrylonitrile/lignin-Based Carbon Nanofibers for High-Power Lithium Ion Battery Anodes. *J. Solid State. Electrochem.* 17, 2471–2475. doi:10.1007/s10008-013-2112-5
- Dupin, J.-C., Gonbeau, D., Vinatier, P., and Levasseur, A. (2000). Systematic XPS Studies of Metal Oxides, Hydroxides and Peroxides. *Phys. Chem. Chem. Phys.* 2, 1319–1324. doi:10.1039/a908800h
- Frey, M. W. (2008). Electrospinning Cellulose and Cellulose Derivatives. *Polym. Rev.* 48, 378–391. doi:10.1080/15583720802022281
- García-Mateos, F. J., Ruiz-Rosas, R., María Rosas, J., Morallón, E., Cazorla-Amorós, D., Rodríguez-Mirasol, J., et al. (2020). Activation of Electrospun Lignin-Based Carbon Fibers and Their Performance as Self-Standing Supercapacitor Electrodes. *Sep. Purif. Tech.* 241, 116724. doi:10.1016/j.seppur.2020.116724
- Guan, L., Yu, L., and Chen, G. Z. (2016). Capacitive and Non-capacitive Faradaic Charge Storage. *Electrochimica Acta* 206, 464–478. doi:10.1016/j.electacta.2016.01.213
- Han, J., Zhang, L. L., Lee, S., Oh, J., Lee, K.-S., Potts, J. R., et al. (2013). Generation of B-Doped Graphene Nanoplatelets Using a Solution Process and Their Supercapacitor Applications. *ACS nano* 7, 19–26. doi:10.1021/nn3034309
- Hérou, S., Crespo Ribadeneyra, M., Schlee, P., Luo, H., Cristian Tanase, L., Roßberg, C., et al. (2021). The Impact of Having an Oxygen-Rich Microporous Surface in Carbon Electrodes for High-Power Aqueous Supercapacitors. *J. Energ. Chem.* 53, 36–48. doi:10.1016/j.jechem.2020.04.068

thanks her UKRI Future Leaders Fellowship (MR/T041412/1) for their support.

## SUPPLEMENTARY MATERIAL

The Supplementary Material for this article can be found online at: <https://www.frontiersin.org/articles/10.3389/fmats.2022.859872/full#supplementary-material>

- Herou, S., Schlee, P., Jorge, A. B., and Titirici, M. (2018). Biomass-derived Electrodes for Flexible Supercapacitors. *Curr. Opin. Green Sust. Chem.* 9, 18–24. doi:10.1016/j.cogsc.2017.10.005
- Hu, S., Zhang, S., Pan, N., and Hsieh, Y.-L. (2014). High Energy Density Supercapacitors from Lignin Derived Submicron Activated Carbon Fibers in Aqueous Electrolytes. *J. Power Sourc.* 270, 106–112. doi:10.1016/j.jpowsour.2014.07.063
- Iranmahboob, J., Hill, D. O., and Toghiani, H. (2001). Characterization of K<sub>2</sub>CO<sub>3</sub>/Co-MoS<sub>2</sub> Catalyst by XRD, XPS, SEM, and EDS. *Appl. Surf. Sci.* 185, 72–78. doi:10.1016/s0169-4332(01)00653-5
- Jeong, J. H., Kim, Y. A., and Kim, B.-H. (2020). Electrospun Polyacrylonitrile/cyclodextrin-Derived Hierarchical Porous Carbon nanofiber/MnO<sub>2</sub> Composites for Supercapacitor Applications. *Carbon* 164, 296–304. doi:10.1016/j.carbon.2020.03.052
- Krittayavathananon, A., Pettong, T., Kidkhunthod, P., and Sawangphruk, M. (2017). Insight into the Charge Storage Mechanism and Capacity Retention Fading of MnCo<sub>2</sub>O<sub>4</sub> Used as Supercapacitor Electrodes. *Electrochimica Acta* 258, 1008–1015. doi:10.1016/j.electacta.2017.11.152
- Kumar, M., Hietala, M., and Oksman, K. (2019). Lignin-Based Electrospun Carbon Nanofibers. *Front. Mater.* 6, 62. doi:10.3389/fmats.2019.00062
- Lai, C., Zhou, Z., Zhang, L., Wang, X., Zhou, Q., Zhao, Y., et al. (2014). Free-standing and Mechanically Flexible Mats Consisting of Electrospun Carbon Nanofibers Made from a Natural Product of Alkali Lignin as Binder-free Electrodes for High-Performance Supercapacitors. *J. Power Sourc.* 247, 134–141. doi:10.1016/j.jpowsour.2013.08.082
- Laudenslager, M. J., Scheffler, R. H., and Sigmund, W. M. (2010). Electrospun Materials for Energy Harvesting, Conversion, and Storage: A Review. *Pure Appl. Chem.* 82, 2137–2156. doi:10.1351/pac-con-09-11-49
- Lei, D., Li, X.-D., Seo, M.-K., Khil, M.-S., Kim, H.-Y., and Kim, B.-S. (2017). NiCo<sub>2</sub>O<sub>4</sub> Nanostructure-Decorated PAN/lignin Based Carbon Nanofiber Electrodes with Excellent Cyclability for Flexible Hybrid Supercapacitors. *Polymer* 132, 31–40. doi:10.1016/j.polymer.2017.10.051
- Li, X.-R., Jiang, Y.-H., Wang, P.-Z., Mo, Y., Lai, W.-D., Li, Z.-J., et al. (2020). Effect of the Oxygen Functional Groups of Activated Carbon on its Electrochemical Performance for Supercapacitors. *New Carbon Mater.* 35, 232–243. doi:10.1016/s1872-5805(20)60487-5
- Li, X.-Y., Yan, Y., Zhang, B., Bai, T.-J., Wang, Z.-Z., and He, T.-S. (2021). PAN-derived Electrospun Nanofibers for Supercapacitor Applications: Ongoing Approaches and Challenges. *J. Mater. Sci.* 56, 10745–10781. doi:10.1007/s10853-021-05939-6
- Li, X., Chen, Y., Huang, H., Mai, Y.-W., and Zhou, L. (2016). Electrospun Carbon-Based Nanostructured Electrodes for Advanced Energy Storage - A Review. *Energ. Storage Mater.* 5, 58–92. doi:10.1016/j.ensm.2016.06.002
- Ma, C., Li, Z., Li, J., Fan, Q., Wu, L., Shi, J., et al. (2018). Lignin-based Hierarchical Porous Carbon Nanofiber Films with superior Performance in Supercapacitors. *Appl. Surf. Sci.* 456, 568–576. doi:10.1016/j.apsusc.2018.06.189
- Ma, X., Kolla, P., Zhao, Y., Smirnova, A. L., and Fong, H. (2016). Electrospun Lignin-Derived Carbon Nanofiber Mats Surface-Decorated with MnO<sub>2</sub> Nanowhiskers as Binder-free Supercapacitor Electrodes with High Performance. *J. Power Sourc.* 325, 541–548. doi:10.1016/j.jpowsour.2016.06.073
- Mao, X., Hatton, T., and Rutledge, G. (2013). A Review of Electrospun Carbon Fibers as Electrode Materials for Energy Storage. *Coc* 17, 1390–1401. doi:10.2174/1385272811317130006
- Mikeš, P., Baker, D. A., Uhlin, A., Lukáš, D., Kuželová-Košťáková, E., Vidrich, A., et al. (2021). The Mass Production of Lignin Fibres by Means of Needleless

- Electrospinning. *J. Polym. Environ.* 29, 2164–2173. doi:10.1007/s10924-020-02029-7
- Min, B.-M., Lee, S. W., Lim, J. N., You, Y., Lee, T. S., Kang, P. H., et al. (2004). Chitin and Chitosan Nanofibers: Electrospinning of Chitin and Deacetylation of Chitin Nanofibers. *Polymer* 45, 7137–7142. doi:10.1016/j.polymer.2004.08.048
- Moerck, R. Y., Kringstad, K. P., and Hatakeyama, H. (1987). Fractionation of Kraft Lignin by Successive Extraction with Organic Solvents. 1. Functional Groups (13C-NMR-Spectra and Molecular Weight Distributions. *Holzforschung* 40, 51–60.
- Naseri, F., Karimi, S., Farjah, E., and Schaltz, E. (2022). Supercapacitor Management System: A Comprehensive Review of Modeling, Estimation, Balancing, and protection Techniques. *Renew. Sust. Energ. Rev.* 155, 111913. doi:10.1016/j.rser.2021.111913
- Perera Jayawickramage, R. A., Balkus, K. J., and Ferraris, J. P. (2019). Binder Free Carbon Nanofiber Electrodes Derived from Polyacrylonitrile-Lignin Blends for High Performance Supercapacitors. *Nanotechnology* 30, 355402. doi:10.1088/1361-6528/ab2274
- Poursorkhabi, V., Abdelwahab, M. A., Misra, M., Khalil, H., Gharabaghi, B., and Mohanty, A. K. (2020). Processing, Carbonization, and Characterization of Lignin Based Electrospun Carbon Fibers: A Review. *Front. Energ. Res.* 8, 208. doi:10.3389/fenrg.2020.00208
- Sadezky, A., Muckenhuber, H., Grothe, H., Niessner, R., and Pöschl, U. (2005). Raman Microspectroscopy of Soot and Related Carbonaceous Materials: Spectral Analysis and Structural Information. *Carbon* 43, 1731–1742. doi:10.1016/j.carbon.2005.02.018
- Schlee, P., Herou, S., Jervis, R., Shearing, P. R., Brett, D. J. L., Baker, D., et al. (2019). Free-standing Supercapacitors from Kraft Lignin Nanofibers with Remarkable Volumetric Energy Density. *Chem. Sci.* 10, 2980–2988. doi:10.1039/c8sc04936j
- Smith, M., Scudiero, L., Espinal, J., Mcewen, J.-S., and Garcia-Perez, M. (2016). Improving the Deconvolution and Interpretation of XPS Spectra from Chars by Ab Initio Calculations. *Carbon* 110, 155–171. doi:10.1016/j.carbon.2016.09.012
- Suda, Y., Mizutani, A., Harigai, T., Takikawa, H., Ue, H., and Umeda, Y. (2017). Influences of Internal Resistance and Specific Surface Area of Electrode Materials on Characteristics of Electric Double Layer Capacitors. *AIP Conf. Proc.* 1807, 020022. doi:10.1063/1.4974804
- Sun, J., Wu, M., Jiang, H., Fan, X., and Zhao, T. (2021). Advances in the Design and Fabrication of High-Performance Flow Battery Electrodes for Renewable Energy Storage. *Adv. Appl. Energ.* 2, 100016. doi:10.1016/j.adapen.2021.100016
- Svinterikos, E., Zuburtikudis, I., and Al-Marzouqi, M. (2020). Electrospun Lignin-Derived Carbon Micro- and Nanofibers: A Review on Precursors, Properties, and Applications. *ACS Sust. Chem. Eng.* 8, 13868–13893. doi:10.1021/acsschemeng.0c03246
- Szewczyk, P. K., Gradys, A., Kim, S. K., Persano, L., Marzec, M., Kryshal, A., et al. (2020). Enhanced Piezoelectricity of Electrospun Polyvinylidene Fluoride Fibers for Energy Harvesting. *ACS Appl. Mater. Inter.* 12, 13575–13583. doi:10.1021/acsami.0c02578
- Tiwari, A. P., Mukhiya, T., Muthurasu, A., Chhetri, K., Lee, M., Dahal, B., et al. (2021). A Review of Electrospun Carbon Nanofiber-Based Negative Electrode Materials for Supercapacitors. *Electrochem* 2, 236–250. doi:10.3390/electrochem2020017
- Vicentini, R., Da Silva, L. M., Franco, D. V., Nunes, W. G., Fiates, J., Doubek, G., et al. (2021). Raman Probing Carbon & Aqueous Electrolytes Interfaces and Molecular Dynamics Simulations towards Understanding Electrochemical Properties under Polarization Conditions in Supercapacitors. *J. Energ. Chem.* 60, 279–292. doi:10.1016/j.jechem.2021.01.003
- Wang, L., Gele, A., and Sun, Y. (2017). Preparation of Iron Oxide Particle-Decorated Lignin-Based Carbon Nanofibers as Electrode Material for Pseudocapacitor. *J. Wood Chem. Tech.* 37, 423–432. doi:10.1080/02773813.2017.1310900
- Wang, X., Zhang, W., Chen, M., and Zhou, X. (2018). Electrospun Enzymatic Hydrolysis Lignin-Based Carbon Nanofibers as Binder-free Supercapacitor Electrodes with High Performance. *Polymers (Basel)* 10, 1306. doi:10.3390/polym10121306
- Wen, Y., Kok, M. D. R., Tafoya, J. P. V., Sobrido, A. B. J., Bell, E., Gostick, J. T., et al. (2021). Electrospinning as a Route to Advanced Carbon Fibre Materials for Selected Low-Temperature Electrochemical Devices: A Review. *J. Energ. Chem.* 59, 492–529. doi:10.1016/j.jechem.2020.11.014

**Conflict of Interest:** The authors declare that the research was conducted in the absence of any commercial or financial relationships that could be construed as a potential conflict of interest.

**Publisher's Note:** All claims expressed in this article are solely those of the authors and do not necessarily represent those of their affiliated organizations, or those of the publisher, the editors and the reviewers. Any product that may be evaluated in this article, or claim that may be made by its manufacturer, is not guaranteed or endorsed by the publisher.

Copyright © 2022 Thielke, Lopez Guzman, Victoria Tafoya, García Tamayo, Castro Herazo, Hosseinaei and Sobrido. This is an open-access article distributed under the terms of the Creative Commons Attribution License (CC BY). The use, distribution or reproduction in other forums is permitted, provided the original author(s) and the copyright owner(s) are credited and that the original publication in this journal is cited, in accordance with accepted academic practice. No use, distribution or reproduction is permitted which does not comply with these terms.